Nonlinear spectral management: Linearization of the lossless fiber channel

Jaroslaw E. Prilepsky,[1,*] **Stanislav A. Derevyanko,**[1,2] **and Sergei K. Turitsyn**[1]

[1]*Aston Institute of Photonic Technologies, Aston University, B4 7ET Birmingham, UK*
[2]*Department of Physics of Complex Systems, Weizmann Institute of Science, Rehovot 76100, Israel*
[*]*y.prylepskiy1@aston.ac.uk*

Abstract: Using the integrable nonlinear Schrödinger equation (NLSE) as a channel model, we describe the application of *nonlinear spectral management* for effective mitigation of all nonlinear distortions induced by the fiber Kerr effect. Our approach is a modification and substantial development of the so-called "eigenvalue communication" idea first presented in A. Hasegawa, T. Nyu, J. Lightwave Technol. **11**, 395 (1993). The key feature of the nonlinear Fourier transform (inverse scattering transform) method is that for the NLSE, any input signal can be decomposed into the so-called scattering data (nonlinear spectrum), which evolve in a trivial manner, similar to the evolution of Fourier components in linear equations. We consider here a practically important weakly nonlinear transmission regime and propose a general method of the effective encoding/modulation of the nonlinear spectrum: The machinery of our approach is based on the recursive Fourier-type integration of the input profile and, thus, can be considered for electronic or all-optical implementations. We also present a novel concept of nonlinear spectral pre-compensation, or in other terms, an effective nonlinear spectral pre-equalization. The proposed general technique is then illustrated through particular analytical results available for the transmission of a segment of the orthogonal frequency division multiplexing (OFDM) formatted pattern, and through WDM input based on Gaussian pulses. Finally, the robustness of the method against the amplifier spontaneous emission is demonstrated, and the general numerical complexity of the nonlinear spectrum usage is discussed.

© 2013 Optical Society of America

OCIS codes: (060.1660) Coherent communications; (060.2330) Fiber optics communications; (070.4340) Nonlinear optical signal processing.

References and links

1. A. Hasegawa and Y. Kodama, *Solitons in Optical Communications* (Oxford University Press, 1995).
2. G. P. Agrawal, *Nonlinear Fiber Optics*, 4th ed. (Elsevier, 2006).
3. J. P. Gordon and L. F. Mollenauer, "Phase noise in photonic communications systems using linear amplifiers," Opt. Lett. **15**, 1351–1353 (1990).
4. A. Mecozzi, "Limits to the long haul coherent transmission set by the Kerr nonlinearity and noise of in-line amplifiers," J. Lightwave Technol. **12**, 1993-2000 (1994).
5. P. P. Mitra and J. B. Stark, "Nonlinear limits to the information capacity of optical fibre communications," Nature **411**, 1027–1030 (2001).
6. E. B. Desurvire, "Capacity demand and technology challenges for lightwave systems in the next two decades," J. Lightwave Technol. **24**, 4697–4710 (2006).

7. R.-J. Essiambre, G. Foschini, G. Kramer, and P. Winzer, "Capacity limits of information transport in fiber-optic networks," Phys. Rev. Lett. **101**, 163901 (2008).
8. A. D. Ellis, J. Zhao, and D. Cotter, "Approaching the non-linear Shannon limit," J. Lightwave Technol. **28**, 423–433 (2010).
9. D. J. Richardson, "Filling the light pipe," Science **330**, 327–328 (2010).
10. R. I. Killey and C. Behrens, "Shannon's theory in nonlinear systems," J. Mod. Opt. **58**, 1–10 (2011).
11. A. Mecozzi and R.-J. Essiambre, "Nonlinear Shannon limit in pseudo-linear coherent systems," J. Lightwave Technol. **30**, 2011–2024 (2012).
12. K. S. Turitsyn and S. K. Turitsyn, "Nonlinear communication channels with capacity above the linear Shannon limit," Opt. Lett. **37**, 3600–3602 (2012).
13. see *Impact of nonlinearities on fiber-optic communication systems*, Ed. S. Kumar, (Springer, 2011).
14. A. Splett, C. Kurtzke, and K. Petermann, "Ultimate transmission capacity of amplified optical fiber communication systems taking into account fiber nonlinearities," in *Tech. Digest of European Conference on Optical Communication*, 1993, paper MoC2.4.
15. D. Rafique and A. D. Ellis, "Impact of signal-ASE four-wave mixing on the effectiveness of digital back-propagation in 112 Gb/s PM-QPSK systems," Opt. Express **19**, 3449-3454 (2011).
16. E. Ip and J. Kahn, "Compensation of dispersion and nonlinear impairments using digital backpropagation," J. Lightwave Technol. **26**, 3416-3425 (2008).
17. D. S. Millar, S. Makovejs, C. Behrens, S. Hellerbrand, R. I. Killey, P. Bayvel, and S. J. Savory, "Mitigation of fiber nonlinearity using a digital coherent receiver," IEEE J. Sel. Top. Quantum Electron. **16**, 1217–1226 (2010).
18. M. Nazarathy, J. Khurgin, R. Weidenfeld, Y. Meiman, P. Cho, R. Noe, I. Shpantzer, and V. Karagodsky, "Phased-array cancellation of nonlinear FWM in coherent OFDM dispersive multi-span links," Opt. Express **15**, 15777-15810 (2008).
19. S. Shieh and I. Djordjevic, *OFDM for Optical Communications* (Academic Press, 2010).
20. W. Shieh, H. Bao, and Y. Tang, "Coherent optical OFDM: theory and design," Opt. Express **16**, 841–859 (2008).
21. L. B. Y. Du and A. J. Lowery, "Pilot-based XPM nonlinearity compensator for CO-OFDM systems," Opt. Express **19**, B862–B869 (2011).
22. L. B. Du, M. M. Morshed, and A. J. Lowery, "Fiber nonlinearity compensation for OFDM super-channels using optical phase conjugation," Opt. Express **20**, 19921–19927 (2012).
23. X. Liu, A. R. Chraplyvy, P. J. Winzer, R. W. Tkach, and S. Chandrasekhar, "Phase-conjugated twin waves for communication beyond the Kerr nonlinearity limit," Nat. Photonics **7**, 560-568 (2013).
24. H. Cheng, W. Li, Y. Fan, Z. Zhang, S. Yu, and Z. Yang, "A novel fiber nonlinearity suppression method in DWDM optical fiber transmission systems with an all-optical pre-distortion module," Opt. Comm. **290**, 152–157 (2013).
25. V. E. Zakharov and A. B. Shabat, "Exact theory of two-dimensional self-focusing and one-dimensional self-modulation of waves in nonlinear media," Soviet Physics-JETP **34**, 62–69 (1972).
26. M. J. Ablowitz, D. J. Kaup, A. C. Newell, and H. Segur, "The inverse scattering transform-Fourier analysis for nonlinear problems," Stud. Appl. Math. **53**, 249–315 (1974).
27. A. C. Newell, *Solitons in Mathematics and Physics* (SIAM, 1985).
28. V. E. Zakharov, S. V. Manakov, S. P. Novikov, and L. P. Pitaevskii, *Theory of Solitons. The Inverse Scattering Method* (Colsultants Bureau, 1984).
29. M. J. Ablowitz and H. Segur, *Solitons and the Inverse Scattering Transform* (SIAM, 1981).
30. M. I. Yousefi and F. R. Kschischang, "Information transmission using the nonlinear Fourier transform, Part I: Mathematical tools," http://arxiv.org/abs/1202.3653, submitted to IEEE Trans. Inf. Theory, Feb. 2012; "Part II: Numerical methods," Apr. 2012, online: http://arxiv.org/abs/1204.0830, submitted to IEEE Trans. Inf. Theory, Feb. 2012; "Part III: Spectrum modulation," Feb. 2013, online: http://arxiv.org/abs/1302.2875, submitted to IEEE Trans. Inf. Theory, Feb. 2013.
31. D. J. Kaup, "Closure of the squared Zakharov-Shabat eigenstates," J. Math. Anal. Appl. **54**, 849–864 (1976).
32. L. F. Mollenauer and J. P. Gordon, *Solitons in Optical Fibers: Fundamentals and Applications* (Academic Press, 2006).
33. Yu. S. Kivshar and G. P. Agrawal, *Optical Solitons: From Fibers to Photonic Crystals* (Academic Press, 2003).
34. A. Hasegawa and T. Nyu, "Eigenvalue communication," J. Lightwave Technol. **11**, 395-399 (1993).
35. J. E. Prilepsky, S. A. Derevyanko, and S. K. Turitsyn, "Lattice approach to the dynamics of phase-coded soliton trains," J. Phys. A: Math. Theor. **45**, 025202 (2012).
36. J. E. Prilepsky, S. A. Derevyanko, and S. K. Turitsyn, "Temporal solitonic crystals and non-Hermitian informational lattices," Phys. Rev. Lett. **108**, 183902 (2012).
37. J. Satsuma and N. Yadjima, "Initial value problems of one-dimensional self-modulation of nonlinear waves in dispersive media," Progr. Theor. Phys. Suppl. **55**, 284-306 (1974).
38. R. Feced, M. N. Zervas, and M. A. Muriel, "An efficient inverse scattering algorithm for the design of nonuniform fiber Bragg gratings," IEEE J. Quant. Electron. **35**, 1105–1115 (1999).
39. W. Shieh, X. Yi, Y. Ma, and Q. Yang, "Coherent optical OFDM: has its time come? [Invited]," J. Opt. Networking **7**, 234–255 (2008).
40. R. Bouziane, P. Milder, R. Koutsoyannis, Y. Benlachtar, J. C. Hoe, M. Puschel, M. Glick, and R. I. Kille, "Design

studies for ASIC implementations of 28 GS/s optical QPSK- and 16-QAM-OFDM transceivers," Opt. Express **19**, 20857–20864 (2011).

41. S. Herbst, S. Bayer, H. Wernz, and H. Griesser, "21-GHz single-band OFDM transmitter with QPSK modulated subcarriers," in *Optical Fiber Communication Conference and Exposition (OFC/NFOEC), 2011 and the National Fiber Optic Engineers Conference*, IEEE, 2011, paper OMS3.

42. A.H. Gnauk and P. J. Winzer, "Optical phase-shift-keyed transmission," J. Lightwave Technol. **23**, 115–130 (2005).

43. S.V. Manakov, "On nonlinear Fraunhofer diffraction," Soviet Physics-JETP **38**, 693–696 (1974).

44. S. A. Derevyanko and J. E. Prilepsky, "Soliton generation from randomly modulated return-to-zero pulses," Opt. Comm. **281**, 5439-5443 (2008).

45. S. A. Derevyanko and J. E. Prilepsky, "Random input problem for the nonlinear Schrodinger equation," Phys. Rev. E **78**, 046610 (2008).

46. M. Klaus and J. K. Shaw, "Purely imaginary eigenvalues of Zakharov-Shabat systems," Phys. Rev. E **65**, 036607 (2002).

47. J. E. Prilepsky, S. A. Derevyanko, and S. K. Turitsyn, "Conversion of a chirped Gaussian pulse to a soliton or a bound multisoliton state in quasilossless and lossy optical fiber spans," J. Opt. Soc. Am. B **24**, 1254–1261 (2007).

48. S. K. Turitsyn and S. A. Derevyanko, "Soliton-based discriminator of noncoherent optical pulses," Phys. Rev. A **78**, 063819 (2008).

49. S. Vergeles and S. K. Turitsyn, "Optical rogue waves in telecommunication data streams," Phys. Rev. A **83**, 061801(R) (2011).

50. S. K. Turitsyn, M. Sorokina, and S. Derevyanko, "Dispersion-dominated nonlinear fiber-optic channel," Opt. Lett. **37**, 2931–2933 (2012).

51. G. Boffetta and A. R. Osborne, "Computation of the direct scattering transform for the nonlinear Schroedinger equation," J. Comput. Phys. **102**, 252-264 (1992).

52. S. Oda, A. Maruta, and K. Kitayama, "All-Optical Quantization Scheme Based on Fiber Nonlinearity," IEEE Photon. Technol. Lett. **16**, 587–589 (2004).

53. H. Terauchi and A. Maruta, "Eigenvalue Modulated Optical Transmission System Based on Digital Coherent Technology," in *18th OptoElectronics and Communications Conference held jointly with 2013 International Conference on Photonics in Switching (OECC/PS)*, IEICE, 2013, paper WR2-5.

54. O. V. Belai, L. L. Frumin, E. V. Podivilov, and D. A. Shapiro, "Efficient numerical method of the fiber Bragg grating synthesis," J. Opt. Soc. Am. B **24**, 1451–1457 (2007).

55. A. O. Korotkevich and P. M. Lushnikov, " Proof-of-concept implementation of the massively parallel algorithm for simulation of dispersion-managed WDM optical fiber systems," Opt. Lett. **36**, 1851–1853 (2011).

56. M. Van Barel, G. Heinig, and P. Kravanja, "A stabilized superfast solver for nonsymmetric Toeplitz systems," SIAM J. Matrix Anal. Appl. **23**, 494-510 (2001).

57. S. Chandrasekaran, M. Gu. X. Sun, J. Xia, and J. Zhu, "A superfast algorithm for Toeplitz systems of linear equations," SIAM J. Matrix. Anal. Appl. **29**, 1247–1266 (2007).

1. Introduction

Signal transmission down the fiber-optic line is affected simultaneously by several physical phenomena in fibers: dispersion, signal corruption due to the amplifier spontaneous emission, fiber nonlinearity, and other effects [1, 2]. The fiber Kerr nonlinearity is the important feature distinguishing the fiber-channel transmission from the radio-type (open air or space) channel [2]: The dependence of the transmitting media properties on the signal intensity results in a number of detrimental effects produced by the coupling and nonlinear intertwining between the signal degrees of freedom, accompanied by the influence of noise and dispersion. Thus, the data encoded into the signal propagating through the nonlinear channel become corrupt, leading to loss of the transmitted information and decrease in the spectral efficiency of transmission [3–15]. For the suppression of nonlinearity-induced distortions, a number of techniques have been proposed and studied, e.g. digital backpropagation [16], receiver-based digital signal processing [17–20], pilot-based nonlinearity compensator [21], optical [22] and twin-wave [23] phase conjugation, fractional Fourier-based pre-compensation [24], to mention several recent advancements, and many other types of pre-compensation, in-line and post-compensation methods [19,23]. In this work we describe the application of a method (developed a long time ago in the theory of nonlinear evolutionary equations [1, 25–29]) that allows effective linearization of some classes of nonlinear communication channels, to the problem of optical communications.

An important subclass of nonlinear transmission channels is governed by the so-called *integrable* evolutionary equations [1, 25–29]. One of the particular manifestations of this *integrability* property is that given the initial conditions (in the considered context, the waveform of the input signal), we can propagate the signal to a distance L in three steps, which have direct analogies with the same stages in the consideration of linear problems (although the implementation of these steps differs significantly from the linear case). (i) The first step is the mapping of the input profile to the *spectral domain*. For a linear channel, this operation corresponds to the ordinary forward Fourier transform (FT), and according to the already established terminology, we will call this stage the *forward nonlinear Fourier transform (NFT)*, by analogue with the linear situation. For nonlinear propagation, this stage involves solving the specific direct scattering problem associated with an integrable equation and produces a set of *scattering data*, where the particular quantities (continuous spectrum and a set of localized complex eigenvalues, if the latter exists) are then associated with orthogonal nonlinear "normal modes". (ii) The next step is the propagation of the initial spectral distribution (again, a continuous spectrum and complex eigenvalues) to distance L: Here, in both linear and nonlinear cases, the spectrum evolves according to the linear dispersion law, and this operation is usually quite trivial, amounting to the phase rotation of the corresponding decoupled spectral component. We would like to stress that even if the original problem is nonlinear, the nonlinear spectral components evolve without interaction with each other in full analogy with the linear problem, which explains the term "linearization". (iii) The last stage is the recovery of the solution profile in the space-time domain: It is the backward FT in the linear case. For the nonlinear integrable problem, the backward NFT amounts to the solution of the so-called Gelfand-Levitan-Marchenko equations [1, 25–29], and this step accomplishes the finding of a solution (signal profile) at distance L. These three stages which provide the solution of a nonlinear equation at distance L, constitute the method of the inverse scattering transform (IST) [1, 25–29]. Another important aspect of the NFT [1, 25–30] is that, due to effective linearization of the channel, all nonlinear propagation effects such as self-phase modulation, cross phase modulation, and four-wave mixing are effectively removed owing to the orthogonality property of the nonlinear spectrum (NS) components (involving both discrete (soliton) and continuous spectrum) [31], thus removing the very reason for the spectral efficiency decay at high signal power. In engineering terms, the NFT method can be treated as effective nonlinear orthogonal frequency division multiplexing [30]. In practical terms, the usage of NS is a novel approach to combat the nonlinear distortions, being an alternative/addition to the commonly used engineering techniques (see e.g. [16, 17, 19, 20, 22–24] and references therein).

The evolution of the slow-varying optical field envelope in a passive optical single-mode fiber is described by the nonlinear Schrödinger equation (NLSE) [1, 2, 32, 33], which introduces the effects of the mutual counteraction of dispersion and nonlinearity. In the absence of losses and external actions, the NLSE is *integrable*, and so the explicit form for the three aforementioned operations (forward/backward NFT and the spectrum evolution law) is known [25]. Since we can decompose the input signal into analogues of orthogonal Fourier modes by performing the forward NFT operation, the dynamics of the signal through the NLSE channel can be completely described by the evolution of these orthogonal modes [1, 25–29], and then, the informational content encoded at the transmitter can be potentially recovered at the receiver without distortions.

The quest for the optimal design of a nonlinear transmission channel and usage of the nonlinearity in a 'constructive' way has occupied researchers for a long time. This includes soliton transmission techniques, dispersion management (e.g. dispersion-managed soliton) for mitigation of nonlinear impairments, optical regeneration, and other approaches. The idea of manipulating the robust NS of NLSE for the purposes of optical transmission was already put

forward nearly 20 years ago [34] and has been intensively scrutinized recently in [30]. Notably, in the original study [34], only the soliton part of the nonlinear spectrum was considered (and these ideas were advanced further in [30]) and no practical fiber optical implementation scheme was suggested. The solitons are described by the localized (complex) eigenvalues of the corresponding spectral problem defining NS. These eigenvalues are the conserved quantities: Their particular magnitudes emerge directly from the parameters of the input profile (encoded signal) and do not change during the propagation. Therefore, these eigenvalues (or even the total number of discrete eigenvalues) can be utilized for encoding and transferring the information, owing to their conservation. However, the usage of pure solitons for transmission purposes has a number of challenges, e.g., the soliton collision problems in WDM systems, low symbol rates etc. [2, 32], although this direction has been revived recently [35, 36] through plugging in the multilevel modulation formats and using coherent transmission with the subsequent effective increase in the transmission rate.

We would like to point out that the direct implementation of the transmission based on the NS brings about significant technical challenges. First, there is no fully developed electronic or optical scheme that could perform forward/backward NFT *without the computer processing of the signal*. Second, the properties of the NS can be significantly different from its linear counterpart, and therefore, if one deals with the "conventional" linear formats, no general method for encoding and recovery of the information exists: Each particular configuration of the NS emerging from the input signal should be studied from scratch, as the NS is a nonlinear functional of the input. Even the number of analytically solvable cases for the forward NFT is very limited [37]. Thus, the principal possibility of NLSE channel linearization should not create any wrong impression, digressing one from the hurdles and challenges in the practical implementation of this technique.

The major goal of the current paper is to outline some solutions for the aforementioned problems. First, in our study, we withhold the use of solitons (so that we do not deal with the discrete part of the NS), thus disposing of the problems associated with the soliton WDM collisions, etc. In this paper, we propose to utilize the *continuous part of the NS* for information encoding and transmission. As mentioned earlier, the advantage of using NS in the integrable NLSE channel is that the nonlinear modes of the continuous NS part are still orthogonal and evolve according to the linear dispersion law: The NS coding is free from the "coupling" nonlinearity influence allowing virtually undistorted transmission of initial data provided that the linear dispersion is compensated at the endpoint.

Further, we describe a general method of calculating the continuous NS when the average power of the input signal (localized within the boundaries of a considered time interval) is not very high and nonlinearity can be treated as a perturbation. We show that in this case, the forward NFT can be performed iteratively and that the NS can be computed with a desirable precision in terms of expansion with respect to the input signal power by implementing the Fourier-type recursive integrations, involving only the input signal itself. Note that these operations can already be suggested for the electronic and/or all-optical implementation.

Finally, based on the expansions of the NS, we are able to cancel the "nonlinear" additions of the NS and, thus, can *equalize* the nonlinear and linear spectra by means of nonlinear *pre-distortion* of the input signal. The equalization of the linear and nonlinear spectra after the nonlinear pre-distortion paves the way for the utilization of "linear" methods, such as ordinary FT for information encoding and decoding. This approach is then studied in detail for illustrative purposes in application to a fragment of an OFDM input pattern with the phase-shift keying (PSK) encoding of OFDM coefficients. It is shown that pre-distortion allows one to obtain an almost undistorted initial signal profile at the receiver after winding out the accumulated linear dispersion in the NS. In the case of the OFDM input, the pre-distortion amounts to

the extraction of the lowest-order terms associated with the inter-carrier (IC) and inter-slot (IS) interference effects.

Our paper is organized as follows. First, in Section 2, we introduce the NLSE and the associated normalizations, determining the scales of the entering parameters, and provide the details of the forward NFT, explaining the relevant quantities characterizing the NS (i.e., we present the elements of the direct scattering problem associated with the NLSE). Section 3 deals with the *general theory of NS* when the amplitude of the input signal is sufficiently low: We present the expression of the NS in terms of the signal amplitude series. Subsection 3.2 explains how these results can be geared for the *effective equalization of the linear and nonlinear spectra*, used further for our *nonlinear pre-distortion method*. In Section 4, we consider the NFT for the OFDM-type inputs. First, in Subsection 4.1, we remind the basics of the OFDM format. After that, in Subsection 4.2, we derive the analytic form of the NS for a single OFDM tone with a finite base extent, and in Subsection 4.3, we mention some general properties of NS associated with the OFDM-type input. Section 5 deals with the direct application of our spectra equalization method. First, we consider the pre-distortion of a single OFDM tone (Subsection 5.1). Then, Subsection 5.2 contains the results for the pre-compensation of a sequence of OFDM-coded slots. Section 6 contains the extension of our approach and discusses how to deal with the situation where the recursive spectra equalization is not effective. First, in Subsection 6.1 we consider precompensation of the input in the form of Gaussian-based WDM pulse and show, that our method is applicable in this case as well. In Subsection 6.2 we analyze the robustness of our method against the amplifier spontaneous emission (ASE). Finally, in Subsection 6.3 we present the estimation of the numerical complexity of the methods based on NFT as compared to digital back-propagation and outline the way of how to further extend the ideas of NFT-based transmission. Our findings are summarized in the Conclusion.

Throughout the paper, we adopt the following conventions for the linear forward/backward FT:

$$Q(\omega) = \int\limits_{-\infty}^{\infty} q(t)\, e^{-i\omega t} dt, \qquad q(t) = \frac{1}{2\pi} \int\limits_{-\infty}^{\infty} Q(\omega)\, e^{i\omega t} d\omega. \tag{1}$$

The overline, e.g. $\bar{q}(t)$, will mark the complex conjugation of the corresponding quantity. The frequency in the linear FT is denoted as ω, and the analogous variable referring to the nonlinear spectral domain is ξ.

2. The model, normalizations, and NFT basics

2.1. NLSE and normalizations

To illustrate key ideas, we consider as a master model the NLSE governing the propagation of a complex slow-varying optical field envelope $q(z,t)$ along a single-mode optical fiber [1, 2, 33]:

$$iq_z - \frac{\beta_2}{2} q_{tt} + \gamma q |q|^2 = 0, \tag{2}$$

where z stands for the propagation distance and t is the time in the frame co-moving with the group velocity of the envelope. Here, we focus on the case of anomalous dispersion (i.e., the constant chromatic dispersion coefficient $\beta_2 < 0$ in Eq. (2)) and hence deal with the so-called *focusing* type of NLSE. We take the typical value of $\beta_2 = -22$ ps^2/km, and the higher-order dispersion terms are not considered here. The instantaneous Kerr nonlinearity coefficient γ is expressed through the nonlinear part of refractive index n_2 and an effective mode area A_{eff}: $\gamma = n_2 \omega_0 / c A_{eff}$, with c being the vacuum speed of light and $\omega_0 = 2\pi v_0$ being the carrier frequency of the envelope $q(t,z)$; the typical value is $\gamma = 1.27$ (W·km)$^{-1}$.

We normalize time in Eq. (2) to the characteristic time related to an input signal T_s, which can be, e.g., the extent of the RZ signal or the duration of a single OFDM slot, and then use the effective z-scale associated with T_s: $Z_s = T_s^2/|\beta_2|$. Then, we measure the power of the input in units of γZ_s and normalize the signal amplitude. The summary of normalizations is as follows

$$\frac{t}{T_s} \to t, \qquad \frac{z}{Z_s} \to z, \qquad q\sqrt{\gamma Z_s} \to q. \qquad (3)$$

Further, we typically assume, without loss of generality, the following values: $T_s \approx 300\text{ps}$, giving the characteristic z normalization scale as $Z_s \approx 4000\text{km}$. For instance, for the typical input peak power of $P_0 \sim 0.1\text{mW}$, the characteristic measure of the effective nonlinearity is $\varepsilon = (\gamma Z_s P_0)^{1/2} \approx 0.5$, and for $P_0 = 1\text{mW}$, $\varepsilon \approx 2.5$

The normalized NLSE (2) is rewritten as

$$iq_z + \frac{1}{2}q_{tt} + q|q|^2 = 0, \qquad (4)$$

where time is measured in units of T_s, distance in units of Z_s, and power of the signal in units of $(\gamma Z_s)^{-1}$.

As mentioned before, the NLSE, Eqs. (2), (4), is integrable by the IST method, i.e., the explicit form of the NFT is known (see below).

2.2. Forward NFT as a part of the IST method

The forward NFT operation for the NLSE (4) requires solutions of the so-called Zakharov-Shabat spectral problem (ZSSP) [1, 25–29], which corresponds to the scattering problem for a non-Hermitian (in the case of anomalous dispersion) Dirac-type system of equations for two auxiliary functions $\phi_{1,2}(t)$, with the NLSE input pulse profile $q(0,t) \equiv q(t)$ serving as an effective *potential* entering the equations

$$\frac{d\phi_1}{dt} = q(t)\phi_2 - i\zeta\phi_1, \qquad \frac{d\phi_2}{dt} = -\bar{q}(t)\phi_1 + i\zeta\phi_2. \qquad (5)$$

Here, ζ is a (generally complex) eigenvalue, $\zeta = \xi + i\eta$, and the potential $q(t)$ is supposed to decay as $t \to \pm\infty$ (see the specific constraints imposed on $q(t)$ decay in [1, 25, 29]).

At the left end $t \to -\infty$ we fix the "initial" condition for the incident wave scattered by the potential $q(t)$ to have the so-called Jost solution $\vec{\Phi}(t, \zeta) = [\phi_1(t, \zeta), \phi_2(t, \zeta)]^T$:

$$\vec{\Phi}(t, \zeta)\Big|_{t \to -\infty} = \begin{pmatrix} 1 \\ 0 \end{pmatrix} \exp(-i\zeta t).$$

With this initial condition, at the right end, $t \to +\infty$, we define two Jost scattering coefficients, $a(\zeta)$ and $b(\zeta)$, constituting the essence of the forward NFT:

$$a(\zeta) = \lim_{t \to \infty} \phi_1(t, \zeta), \exp(i\zeta t), \qquad b(\zeta) = \lim_{t \to \infty} \phi_2(t, \zeta)\exp(-i\zeta t), \qquad (6)$$

with $\phi_{1,2}$ being the corresponding elements of vector $\vec{\Phi}(t, \zeta)$. The (right) reflection coefficient associated with Eq. (5) is then defined as

$$r(\xi) = \frac{b(\xi)}{a(\xi)} = \lim_{t \to \infty} \frac{\phi_2(\zeta, t)}{\phi_1(\zeta, t)} \exp(-2i\zeta t). \qquad (7)$$

The forward NFT operation corresponds to the mapping of the initial field, $q(0,t) = q(t)$, onto the set of *scattering data*:

$$\Sigma = \left[r(\xi), \, \xi \in \mathrm{R}, \quad \left\{ \zeta_n, C_n \equiv \frac{b(\zeta_n)}{a'(\zeta_n)} \right\} \right], \qquad (8)$$

where index n runs over all discrete eigenvalues of ZSSP Eq. (5) (if these are present). The quantity $r(\xi)$ from Eqs. (7), (8) defined for real ξ ("frequency") plays the role of the continuous nonlinear spectral distribution, while the quantities associated with discrete eigenvalues describe solitonic degrees of freedom and do not have analogues in the linear problems. In our case, we deal with the situation where *no solitons are present*, and therefore, the ZSSP (5) does not contain a discrete eigenspectrum:

$$\Sigma = [r(\xi),\ \xi \in \text{Re}],\tag{9}$$

i.e., the *complete* scattering data consist only of the quantity $r(\xi)$.

The backward NFT maps the scattering data Σ onto the space-time domain and requires the solution of the Gelfand-Levitan-Marchenko (GLM) system of equations [1, 25, 29] associated with a particular Σ. However, for the method explained in the beginning of the paper we need only the forward NFT, so that we postpone the discussion of backward NFT to Section 6.3.

The evolution of the reflection coefficient is given by [1, 25, 29]

$$R(L,\xi) = r(\xi)\exp(2i\xi^2 L),\tag{10}$$

where $R(L,\xi)$ is the value of the coefficient after the propagation distance L, and $r(\xi)$ is its initial value determined by Eq. (7), i.e. via solving the ZSSP (5) where the input profile serves as a potential. From Eq. (10), one can see that the NS obeys the linear dispersion law of NLSE (4) if one associates the linear frequency ω with the quantity ξ as $\xi = -\omega/2$. Indeed, from the IST theory, it is known [29] that asymptotically in the linear limit $|q(t)| \to 0$, the following formula is valid:

$$r(\xi) = -\bar{Q}(-2\xi),\tag{11}$$

where $Q(...)$ identifies the ordinary forward FT of the signal $q(t)$ defined in Eq. (1). In view of Eq. (11), it is useful to define the *spectral function* $N(\omega)$ associated with forward NFT via the reflection coefficient:

$$N(\omega) = -\bar{r}(\xi)\Big|_{\xi=-\frac{\omega}{2}}.\tag{12}$$

The obvious benefit of such a definition is that in the linear limit, the NFT transform (12) coincides with its linear counterpart. Further, the term NS implies the spectral function $N(\omega)$ defined in Eq. (12), rather than the reflection coefficient $r(\xi)$ itself.

3. Expansions for the low signal amplitude $\varepsilon \ll 1$ and the concept of spectra equalization

In this section we first, considering the amplitude of the input signal $|q(t)| \sim \varepsilon$ to be small, derive the expansion for the reflection coefficient $r(\xi)$ in terms of ε. Note that the results given in Subsection 3.1 below *are general* and do not imply any specific modulation format. In fact, the only limitation of the method is the relative smallness of the input signal power, given by ε. The smallness of ε allows one to obtain the desired expression using perturbation theory, similar to that used in [38] in the context of the fiber Bragg gratings design. After that, for the sake of illustration and outlining how the method can be applied to specific formats, we successively consider the application of the results obtained to a single tone of OFDM, a single slot of OFDM, and several OFDM slots serving as the NLSE input.

3.1. NFT in the case of a weak nonlinearity (small enough input signal power)

We start with Eqs. (5) looking for the solution expansion in terms of the scattering data (the situation is analogous to the expansion of the trajectory integrals [38]).

First, one makes the transformation to the slow varying functions $\varphi_{1,2}$ as: $\varphi_{1,2} = e^{\mp i\xi t}\phi_{1,2}$. In terms of $\varphi_{1,2}$, the expression for $r(\xi)$ (7) now changes to

$$r(\xi) = \lim_{t \to \infty} \frac{\varphi_2(\xi,t)}{\varphi_1(\xi,t)}. \tag{13}$$

Substituting these functions, $\varphi_{1,2}$, in Eqs. (5), we arrive at the system

$$\frac{d\varphi_1}{dt} = e^{2i\xi t}q(t)\varphi_2, \qquad \frac{d\varphi_2}{dt} = -e^{-2i\xi t}\bar{q}(t)\varphi_1, \tag{14}$$

with the transformed initial condition: $[\varphi_1(-T/2,\xi), \varphi_2(-T/2,\xi)] = [1,0]$ (recall that we assume the finite extent of the input as $[-T/2, T/2]$). Then, we express the solution of the second equation from set (14) as

$$\varphi_2(t,\xi) = -\int_{-T/2}^{t} dt_1\, e^{-2i\xi t_1}\bar{q}(t_1)\varphi_1(t_1,\xi), \tag{15}$$

and the solution of the first one as

$$\varphi_1(t,\xi) = 1 + \int_{-T/2}^{t} dt_2\, e^{2i\xi t_2}q(t_2)\varphi_2(t_2,\xi). \tag{16}$$

Now, we substitute Eq. (15) into Eq. (16) and vise versa recursively to obtain the following expansions:

$$\varphi_2(t,\xi) = -\int_{-T/2}^{t} dt_1\, e^{-2i\xi t_1}\bar{q}(t_1) + \int_{-T/2}^{t} dt_1 \int_{-T/2}^{t_1} dt_2 \int_{0}^{t_2} dt_3\, e^{2i\xi(t_2-t_1-t_3)}\bar{q}(t_1)q(t_2)\bar{q}(t_3), \tag{17}$$

up to ε^3 (each power of q gives the contribution $\sim \varepsilon$), and

$$\varphi_1(t,\xi) = 1 - \int_{-T/2}^{t} dt_1 \int_{-T/2}^{t_1} dt_2\, e^{2i\xi(t_1-t_2)}q(t_1)\bar{q}(t_2), \tag{18}$$

up to ε^2. Note that this recursion can be used for obtaining the Jost coefficients $a(\xi)$ and $b(\xi)$ separately up to a desired precision.

The expression for $r(\xi)$ takes the form $r \approx r_0(\xi) + r_1(\xi)$, where $r_0 \sim \varepsilon$ and $r_1 \sim \varepsilon^3$ are given as follows (the next term in this expansion is $\sim \varepsilon^5$):

$$r_0(\xi) = -\int_{-T/2}^{T/2} dt_1\, e^{-2i\xi t_1}\bar{q}(t_1), \tag{19}$$

$$r_1(\xi) = -\int_{-T/2}^{T/2} dt_1 \int_{t_1}^{T/2} dt_2 \int_{-T/2}^{t_2} dt_3\, e^{2i\xi(t_2-t_1-t_3)}\bar{q}(t_1)q(t_2)\bar{q}(t_3). \tag{20}$$

Now we "propagate" our $r(\xi)$ to the distance L using Eq. (10)

$$R(L,\xi) = R_0(L,\xi) + R_1(L,\xi) = [r_0(\xi) + r_1(\xi)]e^{2i\xi^2 L}, \tag{21}$$

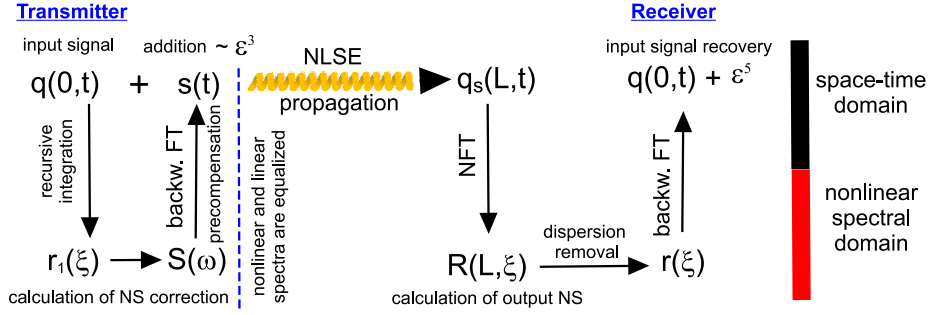Fig. 1. The flowchart of the precompensation scheme for the equalization of the linear and nonlinear spectra up to ε^5 and the subsequent recovery of the informational content encoded at the transmitter.

to obtain the expression for the nonlinear spectral distribution at $z = L$, where $R_0 \sim \varepsilon$ and $R_1 \sim \varepsilon^3$. The direct perturbation theory (i.e. the usage of NLSE (2) itself rather than spectral domain) may also be used for calculation of the NS corrections.

We note, that of course one could also in principle achieve the equalization result without resorting to IST by linearizing NLSE (4) directly in the time domain. Yet when considering the effects of other perturbations on signal propagation (like e.g. ASE noise) the NS-based approach is the best way to go forward. This is due to the very mathematical structure of integrable NLS [28]: The nonlinear spectrum plays the role of so called adiabatic invariants and as such represents a valid basis for any perturbative expansion (as it does not develop secular terms). The NS based approach also provides the correct anzatz for the large distance asymptotes of the NLSE solutions [28].

3.2. Linear and nonlinear spectra equalization using signal pre-distortion

Suppose that at the input $z = 0$, we apply pre-distortion $s(t) \sim \varepsilon^3$ to the initial signal waveform $q(t)$:

$$q_s(t) = q(t) + s(t). \tag{22}$$

The idea of nonlinear pre-distortion is to remove the quantity $r_1(\xi)$ given by Eq. (20) and, thus, the term $R_1(L, \xi)$ from the spectral density at the end point $z = L$ in Eq. (21), by using the additional pre-processing given by $s(t)$. Looking at the form of $r(\xi)$ expansion, we see that when a small quantity $s(t) \sim \varepsilon^3$ is added to the input signal, then we gain a correction $r_s(\xi) \sim \varepsilon^3$ to the expression for $r_1(\xi)$, see Eq. (20):

$$r(\xi) = r_0(\xi) + r_1(\xi) + r_s(\xi) + O(\varepsilon^5),$$

where

$$r_s(\xi) = - \int\limits_{-T/2}^{T/2} dt_1\, e^{-2i\xi t_1} \bar{s}(t_1). \tag{23}$$

For two terms of the same order, $r_1(\xi)$ and $r_s(\xi)$, to cancel each other, we choose $s(t)$ in such a way that the following relation is satisfied:

$$r_s(\xi) = -r_1(\xi). \tag{24}$$

Using the definition of the NS (12), we can now obtain the ordinary Fourier spectrum $S(\omega)$ for our correction $s(t)$ as

$$S(\omega) = \bar{r}_1(\xi)\big|_{\xi=-\frac{\omega}{2}}, \tag{25}$$

and performing the backward FT of Eq. (25), we restore the profile of $s(t)$ in the time domain. Thus, for the predistorted signal $q_s(t) = q(t) + s(t)$ with the FT of $s(t)$ given by Eq. (25), the addition to the nonlinear spectrum $\sim \varepsilon^3$ disappears altogether and *the NS associated with $q_s(t)$ coincides with the linear spectrum of initial $q(t)$* up to the terms $\sim \varepsilon^5$.

The flowchart of the pre-distortion scheme and the signal recovery from the pre-processed NS at distance $z = L$ is given in Fig. 1.

Note that by considering the higher-order nonlinear pre-distortions to $q(t)$, we can cancel the higher terms in the expansion of NS. At the same time, we emphasize that the recursive Fourier-type integration in Eq. (20), used to obtain $r(\xi)$, can be potentially implemented through the electronic or all-optical realization in order to calculate the NS associated with a particular given signal. One of the novel and significant points of our approach is that we are able, by means of precompensation described above, to translate the information encoded in the traditional way in time domain to the nonlinear spectral domain without using any sophisticated special new formats, and control the accuracy of the data mapping. Finally, the transmission itself is effectively performed through the NS evolution.

4. An illustration of the NFT application: OFDM-modulated input signal

4.1. OFDM basics

Coherent optical OFDM (CO-OFDM) has recently become a popular transmission technique owing to its robustness against chromatic dispersion, polarization mode dispersion, and practicality of implementation [19–22, 39, 40]. OFDM is a multi-carrier transmission format where a data stream is carried with many lower-rate sub-carriers (tones):

$$q(t) = \sum_{\alpha=-\infty}^{\infty} \sum_{k=0}^{N_{sc}-1} c_{\alpha k}\, s_k(t - \alpha T)\, e^{i\Omega_k t}. \tag{26}$$

Here, $c_{\alpha k}$ is the α-th informational coefficient in the k-th subcarrier, s_k is the waveform of the k-th subcarrier, N_{sc} is the total number of the sub-carriers, Ω_k is the frequency of the k-th subcarrier, and T is the symbol length. (The Greek indexes α, β, etc., enumerate the slots, while Latin letters indicate the subcarrier numbers). The shape of each subcarrier, $s_k(t)$, is usually a rectangle $\Pi(t)$ of width T and unit height, and such a choice ensures the orthogonality condition

$$\delta_{kl} = \frac{1}{T} \int_0^T s_k(t)\bar{s}_l(t)\, e^{i(\Omega_k - \Omega_l)t}\, dt,$$

which is met as long as the subcarrier frequencies satisfy

$$\Omega_k - \Omega_l = (2\pi/T)m$$

with an integer m. The coefficients $c_{\alpha j}$ are then recovered by an FT of the signal

$$c_{\alpha k} = \frac{1}{T} \int_{\alpha T}^{(\alpha+1)T} q(t)\, e^{-i\Omega_k t}\, dt.$$

This signifies that these orthogonal subcarrier sets, with their frequencies spaced at multiples of the inverse of the symbol rate,

$$\Omega_k = (2\pi/T)(k-1), \tag{27}$$

can be recovered without intercarrier (IC) and interslot (IS) interference, in spite of strong spectral signal overlapping.

The linear spectrum of the OFDM-modulated signal (26) is a comb of sinc-like shapes:

$$Q(\omega) = 2 \sum_{\alpha=-\infty}^{\infty} \sum_{k=1}^{N_{sc}} c_{\alpha k} \exp\left[-i\omega\alpha T + (i/2)(\Omega_k - \omega)T\right] \frac{\sin\left[\frac{(\Omega_k - \omega)T}{2}\right]}{\Omega_k - \omega}. \tag{28}$$

In this work, for illustration purpose, we employ the widely used QPSK encoding of the coefficients $c_{\alpha k}$ [19, 36, 40–42] (without losing the generality of the analytical results), with four allowed phase levels used for encoding the informational content: This means that the absolute value of $c_{\alpha k}$ is the same for each coefficient, $|c_{\alpha k}| = c = $ const., and the phase of each $c_{\alpha k}$ takes four discrete values from the set:

$$\text{Arg}\{c_{\alpha k}\} = 2\pi p/4,$$

with $p = 0, 1, 2, 3$.

4.2. NFT in the case of a single OFDM tone

Let us start with the idealized but analytically solvable case when we have only one OFDM slot of length T (extending, say, from $-T/2$ to $T/2$) with a single encoded coefficient, see Eq. (26), as the input for the NLSE channel. This means that, at $z = 0$, we have the following profile $q(0,t) = q(t)$

$$q(t) = \begin{cases} c_k \exp(i\Omega_k t) & \text{if } t \in \left[-\frac{T}{2}, \frac{T}{2}\right], \\ 0 & \text{otherwise}, \end{cases} \tag{29}$$

to be inserted as a potential into the ZSSP (5). The solution for Eqs. (5) for the potential given by Eq. (29) can obtained analytically using the results for the rectangular pulse [43, 44]:

$$\vec{\Phi}(t+T/2,\xi) = \left(\cos(\xi_k t) - \frac{i\xi_k/2}{\Xi_k}\sin(\Xi_k t)\right)\begin{pmatrix} e^{i\Omega_k t/2} \\ 0 \end{pmatrix} - \frac{\bar{c}_k}{\Xi_k}\sin(\Xi_k t)\begin{pmatrix} 0 \\ e^{-i\Omega_k t/2} \end{pmatrix}, \tag{30}$$

where ξ_k and Ξ_k are the functions of the spectral parameter ξ:

$$\xi_k(\xi) = 2\xi + \Omega_k, \qquad \Xi_k(\xi) = \sqrt{(\xi_k/2)^2 + |c_k|^2}.$$

The reflection coefficient, defining the NS, is then obtained by using Eq. (7):

$$r(\xi) = -\frac{2\bar{c}_k \sin\Xi_k T}{2\Xi_k \cos\Xi_k T - i\xi_k \sin\Xi_k T} \exp\left[-iT\xi_k/2\right]. \tag{31}$$

The nonlinear power spectrum emerging from Eq. (31) is

$$|r(\xi)|^2 = \frac{\cos^2\psi_k \sin^2\Xi_k T}{\cos^2\Xi_k T + \sin^2\psi_k \sin^2\Xi_k T}, \qquad \psi_k = \arctan\frac{\xi_k}{2|c_k|}. \tag{32}$$

4.3. Correspondence between the NS and linear spectrum, soliton creation threshold, and general remarks on the NS associated with the OFDM input

Now, we compare the expression of NS (12), obtained by using reflection coefficient (31) - (32), with the linear FT of a single OFDM slot with a single subcarrier:

$$|Q(\omega)|^2 = 4 |c_k|^2 \frac{\sin^2\left[(\Omega_k - \omega)/2\right]}{(\Omega_k - \omega)^2}. \tag{33}$$

In this particular case, one can check directly the relations (11), (12) by seeking the limiting expression of a single-carrier NS when $|c_k| \to 0$. Indeed, in the limit of a small c_k from Eq. (12) using (31) or (32), one immediately gets Eq. (33).
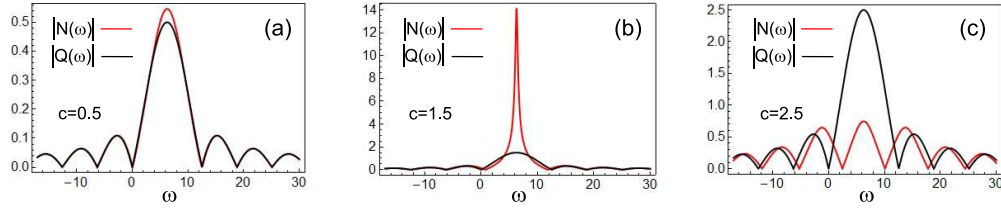

Fig. 2. Dependencies of the absolute value of NS spectral function $|N(\omega)|$, Eq. (12) [red line] and linear spectrum $|Q(\omega)|$, Eq. (33) [black line], calculated for a single tone of OFDM with $\Omega_k = \Omega_2 = 2\pi$ and (normalized) base extent $T = 1$, for the different values of c_k: (a) $c_k = 0.5$; (b) $c_k = 1.5$; (c) $c_k = 2.5$.

In [45], it was demonstrated that the singularities of $r(\xi)$ arising on the real axis ξ due to the increase of the amplitude/length of the signal correspond to the appearance of bound (discrete) states in the ZSSP (5), i.e., bright optical solitons. Such a creation process has a threshold character with respect to both pulse width and amplitude. In the case of a single-carrier OFDM pulse, the amplitude threshold for $|c_k|$ needed for creating the first soliton can be easily obtained from Eq. (32): The expression for $r(\xi)$, Eq. (31), has a singularity when the denominator vanishes, which happens if $\psi_k = 0$ and $\xi_k T = \pi/2$. These two conditions give

$$|c_k|_{th} T = \pi/2, \qquad \xi_{th} = -\frac{\Omega_k}{2}. \tag{34}$$

The threshold value $|c_k|_{th}$ coincides with the well-known *area criterion* (see [29]) for a soliton nucleation, although the latter is strictly valid only for single-hump pulses with a constant phase [46] and is usually violated in the case of chirped inputs [45, 47], where the creation of solitons is significantly suppressed (the latter fact was utilized in the concept of a soliton-based discriminator [48]). In the context of coherent optical communication, due to highly mixed phases of the optical signal resulting from signal overlap from different time slots or from the use of many sub-carriers in OFDM, the phase of an optical signal becomes effectively random [49] and the soliton formation is dramatically suppressed [48]. Note that such a phase mixture together with the signal considered as noise (for technical purposes) can be enhanced by initial pre-dispersion technique [50]. Finally, the value of ξ_{th} gives the position of appearance of the first bound state on the real axis and is related to the velocity of the emerging soliton: $v_{sol} = \Omega_k$.

Now, let us compare the nonlinear and linear spectra of an OFDM tone, i.e., Eq. (31) and the corresponding NS, Eqs. (12) and (33). The comparison is made in Fig. 2, where we plotted an NS (red) and a linear spectrum (black) for different values of the input amplitude. In the

linear case, the main spectral peak corresponds to the single OFDM frequency Ω_k, and the sinc-shape of the spectrum is the consequence of the rectangular pulse-shaping function in the time domain. The NFT spectrum (32) after transformation (12) maintains a similar shape—it is also symmetric with respect to the main peak Ω_k regardless of the value of c_k. The only property that changes drastically is the scaling of the peak with the amplitude. In the linear case it scales as $|c_k|^2$, but in the nonlinear case, it actually scales as $\tan^2(|c_k|T)$, becoming infinite at the threshold $|c_k|_{th}$. So, for the subthreshold c_k, the NS deviates only insignificantly from the linear spectrum, see Fig. 2(a). Then, when we approach $|c_k|_{th}$, we observe an appearance of a pronounced peak indicating the tendency for soliton nucleation, see Fig. 2(b). For the values of c_k beyond the threshold, we already observe the significant structural changes of NS as compared to the linear spectrum, in Fig. 2(c).

For the general form of the OFDM input (26) inserted as a potential in the ZSSP (5), it is impossible to find the analytical expression for the reflection coefficient $r(\xi)$ and, therefore, for the NS (12), as well as for the soliton creation thresholds in terms of the signal extent and amplitude. Moreover, when random values of coefficients entering Eq. (26) are used, each particular realization produces its own NS profile and threshold parameters, and hence, one has to resort to numerical methods [51] for finding the form of NS [see Fig. 3(a)]. However, the conclusions reached above remain qualitatively valid: In the case of low power of the pulse (i.e. below the soliton creation threshold), the NS should have the structure similar to the linear spectrum of the signal (see Fig. 3) with only quantitative deviations, the measure of which is stipulated by how close to the threshold values we are. This fact is used in the next section for performing effective equalization of the NS and linear spectrum by extracting these small deviations between them.

Note that for the chirped and random profiles, the soliton nucleation is strongly suppressed by both the chirp intensity (rapid phase variations) [47] and the incoherence in the input signal [44, 45, 48–50], and one can expect the mitigation of the threshold values (34) produced by a single tone in the case of a multitone randomly coded signal.

In Fig. 3 we also present the results for the dynamics of the linear and nonlinear spectra associated with a fragment of the OFDM input (26): We took 3 slots of the 10-subcarrier OFDM with the pseudo-random QPSK encoding of coefficients for each subcarrier. The extent of each OFDM slot is $T = 1$, and the amplitude of each coefficient is $|c_{\alpha k}| = 0.25$. The case considered produced the subthreshold pattern, i.e., no solitons were nucleated from the input used in our plot. The propagation distance was $z = 1.2$ in normalized units, which corresponds to $L \approx 5000$km for the normalization values described at the end of Subsection 2.1. First, we calculated the NS $N(\omega)$, red line in Figs. 3(a) and 3(b), propagated the input pattern to the distance $z = 1.2$ and again calculated $N(L, \omega)$, blue line in Figs. 3(a) and 3(b) (for the latter case, we removed the linear dispersion). One can see that the NS does not change, which is in accordance with the NS dynamics formula (10): By winding out the linear dispersion corresponding to the distance L, one obtains the exactly initial spectral distribution $N(0, \omega)$ up to the numerical errors associated with the NLSE integration and calculation of NS. In contrast, the profile of $Q(L, \omega)$, green line in Figs. 3(c), 3(d), visibly differs from $Q(0, \omega)$, black line in Figs. 3(c), 3(d), even when we remove the dispersion, because of the nonlinear distortions of the signal during the propagation. Some results for the NS attributed to several other types of input profiles are given in [30].

5. Implementation of the nonlinear pre-distortion

Let us now consider how the general pre-distortion scheme considered above works in a particular case of the OFDM-modulated pulses.
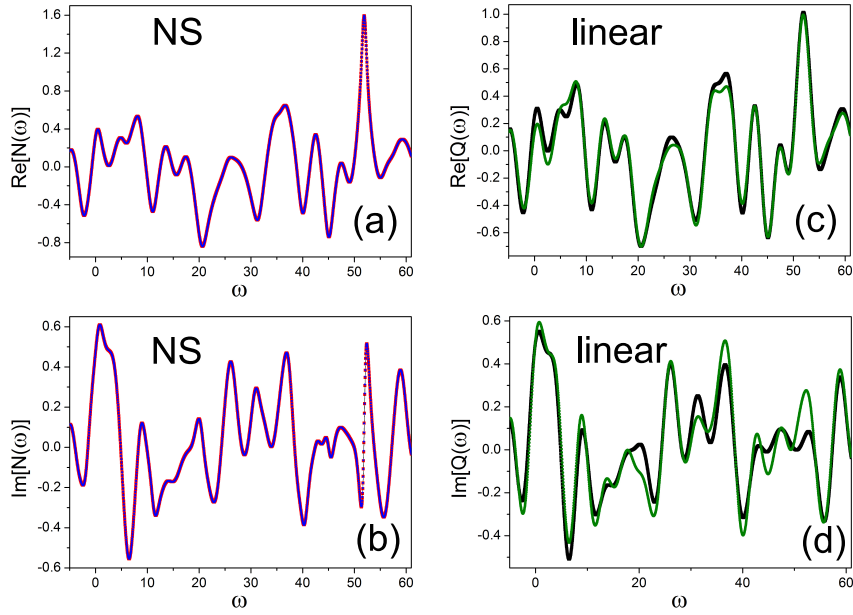
Fig. 3. Nonlinear (a,b) and linear (c,d) spectra for 3 slots of 10-subcarrier QPSK-OFDM before and after the propagation. Panes (a) and (b): the real and imaginary parts of NS $N(\omega)$, for the initial distribution (red) and distribution after the propagation at $z = 1.2$ (i.e. $L \approx 5000$km), blue line. The red and blue parts for $N(\omega)$ are almost indistinguishable insofar as the initial and final NS coincide. Panes (c) and (d): the real and imaginary parts of linear spectrum $Q(\omega)$ for the initial distribution (black) and after the propagation at $z = 1.2$ (i.e. $L \approx 5000$km), green line. For both spectra at $z = 1.2$ (blue and green), the accumulated linear dispersion was removed.

5.1. Pre-distortion of a single OFDM subcarrier in a single time slot

First, we consider the pre-distortion for the input in the form of a single OFDM subcarrier in a single slot given by Eq. (29) having the finite extent $[-\frac{T}{2}, \frac{T}{2}]$ with $|c_k| \sim \varepsilon$ (recall that $\Omega_k = 2\pi(k-1)/T$) [Fig. 4(a)]. Then, we implement the pre-distortion of the NS associated with such an input using the results given in the previous section. Since, in this case, we have the exact analytical expression for the reflection coefficient, Eq. (31), we can simultaneously test the validity of the $r(\xi)$ expansion given in Subsection 3.1. Indeed, one can expand the exact formula (31) in terms of the pulse amplitude c_k to ensure that the general expansion formulas, Eqs. (19) and (20), are correct.

First, for such an input, the first-order NS term is given by

$$r_0(\xi) = -2\bar{c}_k \frac{\sin \xi_k T/2}{\xi_k}, \tag{35}$$

and correspondingly, after the propagation to distance L, the first order-term in the NS expansion is (see Eq. (21))

$$R_0 = -2\bar{c}_k \frac{\sin \xi_k T/2}{\xi_k} e^{2i\xi^2 L}. \tag{36}$$

For the nonlinear addition $\sim \varepsilon^3$, we have

$$r_1(\xi) = 2\bar{c}_k |c_k|^2 \exp\left[i\xi_k T/2\right] \frac{\sin T\xi_k - T\xi_k}{(\xi_k/2)^3}. \tag{37}$$

Note that the expressions above are valid irrespective of the frequency Ω_k value, including the case of an RZ rectangle pulse with $\Omega_1 = 0$ (i.e., the first tone of the OFDM). The magnitude of r_1 (37) at $\xi = -\Omega_k/2$ is $(\varepsilon T)^3$, and therefore, we see that the expansion takes place in terms of the pulse area εT; so, it is actually valid if εT is small.
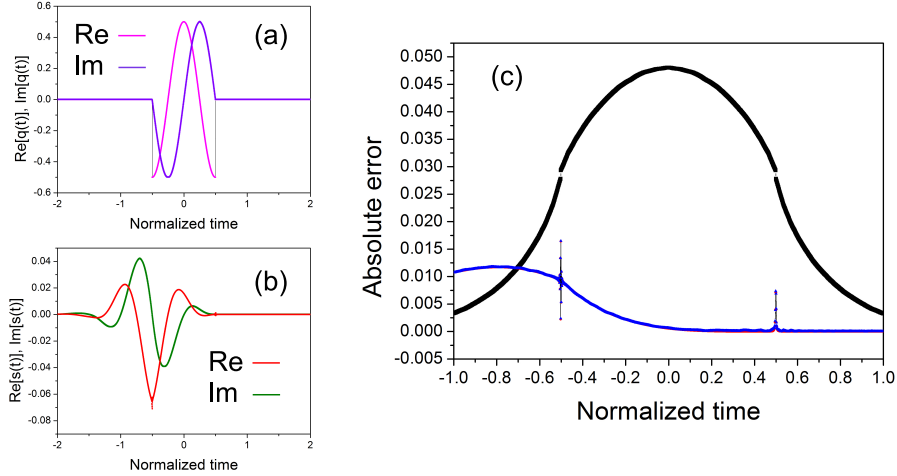

Fig. 4. Pane (a): Real (magenta) and imaginary (purple) parts of the input profile corresponding to a single second OFDM tone with $T = 1$, $\Omega_k = \Omega_2 = 2\pi$, amplitude of the input $c_k = 0.5$. Pane (b): real (dark red) and imaginary (green) parts of the second OFDM tone nonlinear pre-distortion profile $s(t) \sim \varepsilon^3$, given by the backward FT of Eq. (25) with the expression (37) inserted for $r_1(\xi)$. Pane (c): The absolute errors, obtained by the direct integration of NLSE (4) and dispersion removal at at distance $z = 1$ ($L = 4000$km) [black], the usage of the pre-processed NS at the same distance $z = 1$ ($L = 4000$km) [blue] and the (expected) error of the associated with the pre-distorted signal at the input $z = 0$ (red dots, almost indistinguishable). The more detailed explanations of the error definitions are given in the text, see Subsection 5.1
.

Now, we can calculate the pre-distortion correction in the NS domain using Eqs. (24) and the explicit expression (37), and the corresponding correction in the time domain is then obtained by using the backward FT of Eq. (25). The resulting function $s(t)$ is given in Fig. 4(b) for the case $T = 1$, $\varepsilon = 0.5$, where we used the OFDM subcarrier with $k = 2$, i.e., with $\Omega_2 = 2\pi$ [see the profile of $q(t)$ in Fig. 4(a)]. Interestingly, the resulting profile of $s(t)$ is *asymmetric* with respect to time axis origin, in contrast to the obvious symmetry of the input pulse.

In Fig. 4(c), we present the comparison of the absolute errors, $|q(L,t) - q(0,t)|$, for the following three cases.

- First, we numerically calculated the NS $N(\omega)$ for the input given by Eq. (29), predistorted it using Eq. (37), and performed the backward FT to obtain the new preprocessed waveform profile $q_s(0,t)$ in the time domain. Then, we computed the absolute error $|q_s(0,t) - q(t)|$ (red dots, almost indistinguishable on the figures): As expected, the

error is small $\sim c_k^5$. The sharp peaks at the borders of the pulse base are due to the aliasing caused by the abrupt variation of the profile $q(0,t)$.

- Then, we propagated the pre-distorted profile $q_s(0,t)$ to the normalized distance $z = 1$ (corresponding to $L = 4000$km for the normalizations given in Subsection 2.1), thus receiving $q_s(L,t)$. This quantity was used again to compute the NS at distance L, $N(L,\omega)$. After that, we removed linear dispersion from the resulting NS using Eq. (10) and performed the backward FT to obtain $\tilde{q}_s(0,t)$. The absolute error $|\tilde{q}_s(0,t) - q(0,t)|$ in this case is plotted in Fig. 4, represented by blue points. We see that the error almost precisely coincided with the initial error (expected error, red dots), as it should be, with very slight deviations occurring because of numerical errors.

- In the third run, we launched the pure initial profile $q(t)$ without any pre-distortion and then simply removed the linear dispersion after the signal passed the distance $z = 1$, getting the nonlinearity-distorted quantity $\tilde{q}(0,t)$. The black points indicate the absolute error $|\tilde{q}(0,t) - q(t)|$ obtained without the pre-distortion.

Thus, one can see that even in the case of higher numerical errors in the calculation of $R(L,\xi)$ and $N(L,\omega)$, the resulting error (blue) is generally 4-5 times smaller as compared to the case with the simple linear dispersion post-compensation (black). Note that the largest errors for the pre-distorted pulses occurred at the points $t = \pm T/2$, i.e., where we had a sharp change in the input profile: These errors are caused by numerical discretization aliasing.

5.2. Nonlinear pre-distortion of a general finite OFDM-modulated pattern

Now, consider a finite sequence of OFDM slots, each having length T. The input pulse has the form

$$q(t) = \sum_{\alpha=0}^{N_\alpha} \sum_{k=1}^{N_{sc}} c_{\alpha k} \prod (\tau_\alpha, t) \exp(i\Omega_k t), \qquad (38)$$

where α numerates different slots; N_α is the total number of different OFDM slots in our sequence; τ_α indicates the center position for each slot number α; $c_{\alpha k}$ is, as before, the coefficient in the slot α belonging to the k-th OFDM subcarrier; and $\prod(\tau_\alpha, t)$ is the real unit height rectangle profile of the duration T, positioned symmetrically with respect to the point $t = \tau_\alpha$:

$$\prod(\tau_\alpha, t) = \begin{cases} 1 & \text{if } t \in \left[-\frac{T}{2} + \tau_\alpha, \frac{T}{2} + \tau_\alpha \right], \\ 0 & \text{otherwise.} \end{cases}$$

Again, the leading order term in the $r(\xi)$ expansion can be straightforwardly obtained by generalizing Eq. (35):

$$r_0^{\text{OFDM}}(\xi) = \sum_\alpha r_0^\alpha(\xi), \qquad (39)$$

where the partial contributions $r_0^\alpha(\xi)$ are given by

$$r_0^\alpha(\xi) = -2 \sum_k \bar{c}_{\alpha k} \exp(-i\tau_\alpha \xi_k) \frac{\sin \xi_k T/2}{\xi_k}. \qquad (40)$$

In the next order, we have different contributions:

$$\begin{aligned} r_1^{\text{OFDM}}(\xi) &= \sum_\alpha r_1^\alpha(\xi) + \sum_\alpha \sum_{\beta>\alpha} \sum_{\gamma<\beta} r_0^\alpha(\xi)\bar{r}_0^\beta(\xi)r_0^\gamma(\xi) \\ &+ \sum_\alpha \sum_{\gamma<\alpha} r_{12}^\alpha(\xi)r_0^\gamma(\xi) + \sum_\alpha \sum_{\beta>\alpha} r_0^\alpha(\xi)r_{21}^\beta(\xi), \end{aligned} \qquad (41)$$

where $r_1^\alpha(\xi)$ is the contribution from the inter-carrier (IC) interference given by

$$r_1^\alpha(\xi) = \sum_{ijk} \exp(-i\tau_\alpha F_{ijk}) r_{ijk}^{\text{ic}}(\xi). \tag{42}$$

The expression for $r_{ijk}^{\text{ic}}(\xi)$ is

$$\begin{aligned}
r_{ijk}^{\text{ic}}(\xi) = & -2i \frac{c_{\alpha i} \bar{c}_{\alpha j} c_{\alpha k}}{\xi_i \xi_j \xi_k F_{ijk}(\Omega_i - \Omega_j)(\Omega_k - \Omega_j)} \Big[-\bar{E}_k E_j \bar{E}_i \xi_j (\Omega_k - \Omega_j)(\Omega_i - \Omega_j) \\
& -2 E_k \bar{E}_j E_i \xi_k \xi_i (\Omega_k + \Omega_i - 2\Omega_j) + E_k E_j \bar{E}_i \xi_j F_{ijk}(\Omega_k - \Omega_j) \\
& + E_k E_j E_i F_{ijk}(\Omega_i - \Omega_j)(\Omega_k - \Omega_j)/2 + \bar{E}_k E_j E_i \xi_j F_{ijk}(\Omega_i - \Omega_j) \Big],
\end{aligned} \tag{43}$$

with

$$E_i(\xi) = e^{i\xi_i T}, \qquad F_{ijk}(\xi) = 2\xi + \Omega_i - \Omega_j + \Omega_k,$$

and the sums over i, j, and k run from 1 to N_{sc}. It can be easily verified that expression (43) is nonsingular for any ξ. The second term in Eq. (41) is the contribution from the inter-slot (IS) interference, the expression for each partial entry $r_0^{\alpha,\beta,\gamma}(\xi)$ is given by Eq. (40). The two last terms are responsible for the mixed IC/IS interference effects, and the expressions for $r_{12}^\alpha(\xi)$ and $r_{21}^\beta(\xi)$ are given by

$$r_{12}^\alpha(\xi) = i \sum_{i,j} \bar{c}_{\alpha i} c_{\alpha j} \frac{e^{i\tau_\alpha(\Omega_j - \Omega_i)}}{\xi_j} \left(T\delta_{ij} - 2\exp(iT\xi_j/2) \frac{\sin T\xi_i/2}{\xi_i} \right), \tag{44}$$

$$r_{21}^\beta(\xi) = i \sum_{j,k} c_{\beta j} \bar{c}_{\beta k} \frac{e^{i\tau_\beta(\Omega_j - \Omega_k)}}{\xi_k} \left(T\delta_{jk} - 2\exp(iT\xi_k/2) \frac{\sin T\xi_j/2}{\xi_j} \right). \tag{45}$$

Now, using Eqs. (41) and (25), we can calculate the precompensation profile $s(t)$. The absolute errors associated with the propagation of the precompensated OFDM versus the error induced by the nonlinear distortions of the same OFDM sequence are summarized in Fig. 5. We can see that the error is relatively low (notice the aliasing contribution at the ends of each slot) in spite of the extended total duration of the pulse (for the simulation in Fig. 5, we used 3 OFDM slots; so, the duration is now $3T$). This is because the rapid abrupt changes of the OFDM-coded pattern still arrest soliton formation and the NS remains similar to the linear spectrum.

We also checked the preprocessing error for the longer OFDM sequence and found that the precompensation worked relatively well up to 10 OFDM slots with normalized parameters: slot duration $T = 1$ and $|c_{\alpha k}| = 0.1$.

6. Other input profiles, noisy propagation and general comments on NS modulation beyond the perturbative approach.

6.1. Precompensation of other profiles: WDM input with Gaussian base

We have so far considered only OFDM-type input, where the form of NS expansion (20) and the corresponding precompensation profile (23), (25), can be obtained analytically. However, the method described in Section 3 is general and can be applied to arbitrary input forms, with the only requirement that the input pulse does not generate singularities in the NS expansion, i.e., as before, we are far from soliton creation threshold. To give an example of such a situation,
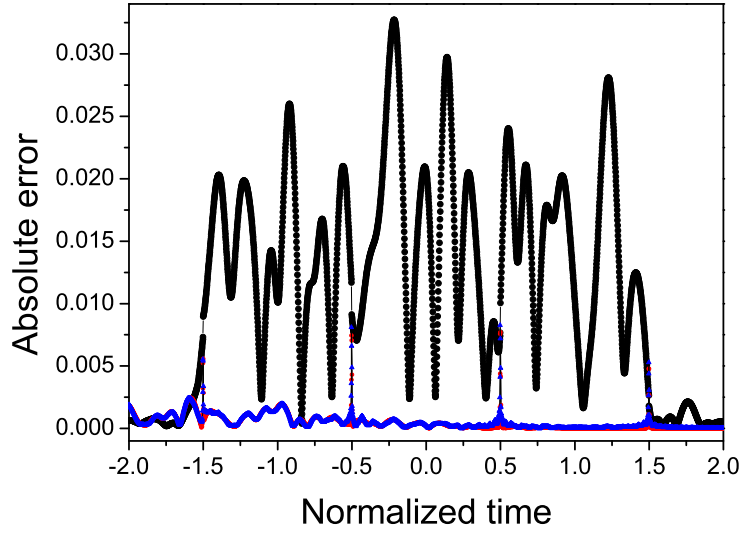
Fig. 5. The absolute errors for the propagation of 3 slots (duration of each slot $T = 1$) of the 10-mode QPSK-OFDM (with the amplitudes of individual coefficients $|c_{\alpha k}| = 0.15$), obtained by the direct dispersion removal at distance $z = 1$ ($L = 4000$km) [black]; the usage of the nonlinear pre-distorted NS at the same distance $z = 1$ ($L = 4000$km) [blue]; and the (expected) error associated with the pre-processed signal at the input $z = 0$ (red, almost indistinguishable). The error definitions are given in Subsection 5.1.

we consider a finite WDM sequence based on Gaussian pulses. The input pulse in this case has the form

$$q(t) = \sum_{\alpha=0}^{N_\alpha} \sum_{k=1}^{N_{ch}} c_{\alpha k} G(\tau_\alpha, \rho, t) \exp(i\Omega_k t), \qquad (46)$$

where, again, α numerates different slots, $G(\tau_\alpha, \rho, t)$ is a Gaussian function centered at τ_α with the (same for each slot) width ρ,

$$G(\tau_\alpha, \rho, t) = \exp\left[-\frac{(t - \tau_\alpha)^2}{\rho^2}\right], \qquad (47)$$

$c_{\alpha k}$ is, as before, the information coefficient in the slot α belonging to the k-th WDM channel of N_{ch} total. For the Gaussian-based WDM input (46) the explicit analytical form of the precompensation profile (25) cannot be obtained, and thus we resort to the numerical procedure [51]: first, we calculate numerically the NS $N(\omega)$ associated with $q(t)$ in the form (46), and then the spectral profile of the pre-compensation correction $S(\omega)$ is given by $S(\omega) = N(\omega) - Q(\omega)$, where $Q(\omega)$ is the linear FT of Eq. (46). The descired pre-compensation profile in the time-domain is given by the backward FT of $S(\omega)$, and, same as it was done in previous sections, one can evaluate the errors associated with the propagation of precompensated input (cf. Fig. 5) and compare them with the errors arising in the propagation without precompensation.

The absolute errors calculated for the propagation of the precompensated Gaussian-based WDM versus the error induced by the nonlinear distortions of the same symbol sequence as in Fig. 5 are summarized in Fig. 6. In the simulation we used 3 slots with the QPSK encoding
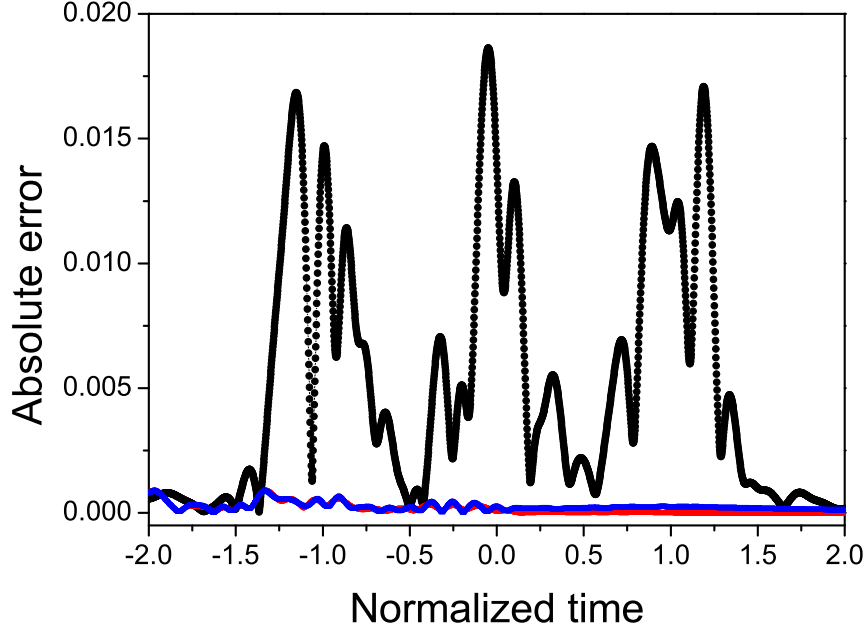
Fig. 6. The absolute errors for the propagation of 3 slots of the 10-mode Gaussian-based QPSK-WDM input (with the amplitudes of individual coefficients $|c_{\alpha k}| = 0.15$), with extent $\rho = 0.3$ (see Eq. (47)), obtained by the direct dispersion removal at distance $z = 1$ ($L = 4000$km) [black]; the usage of the nonlinear precompensated NS at the same distance $z = 1$ ($L = 4000$km) [blue]; and the (expected) error associated with the pre-processed signal at the input $z = 0$ (red, almost indistinguishable). The error definitions are given in Subsection 5.1, normalizations are the same as in Figs. 4, 5.

of $c_{\alpha k}$, the absolute value of each coefficient $c = 0.15$ (cf. Fig. 5); the extent of each Gaussian from (46) is $\rho = 0.3$ (in normalized units), the (normalized) distance between the adjacent Gaussians (slot duration) $\tau_{\alpha+1} - \tau_{\alpha} = 1$. We see that the error now is even lower than that for the QPSK-OFDM with the same parameters, Fig. 5 (the aliasing errors are absent at all since the Gaussians are smooth, in contrast to the rectangular OFDM bases). This is because the Gaussians with $\rho = 0.3$ contain less energy compared to the OFDM with the same parameters, and the remaining terms from the expansions given in Section 3, responsible for the error of the precompensated pulse (i.e. for the difference between the NS and FT), are effectively smaller.

To end up, we see that the spectral equalization method works well for different kinds and power of input profiles provided that the conditions of the validity of expansions from Section 3 are fulfilled.

6.2. *Channel with noise.*

Let us study the robustness of our method against the amplifier spontaneous emission (ASE). In our case we employ the model with distributed Raman amplification, and consider stochastic NLSE [7] with the additive symmetric white Gaussian noise (AWGN) term $\eta(t,z)$:

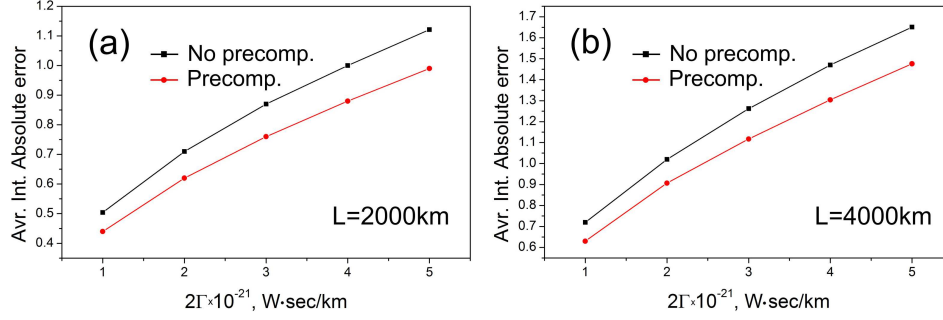$$iq_z - \frac{\beta_2}{2}q_{tt} + \gamma q|q|^2 = \eta(t,z). \tag{48}$$

Fig. 7. The average integral absolute errors for the propagation of 3 slots of the 10-mode QPSK-OFDM input (the parameters are the same as in Fig. 5) in the noisy NLSE, Eq. (48), versus the noise intensity 2Γ, obtained (a) by the direct dispersion removal [black] and the usage of the nonlinear precompensated NS at distance $L = 2000$km [red]; (b) - the same for the propagation distance $L = 4000$km. The averaging for each point was made over 50 realizations.

Here the parameters are the same as in Subsection 2.1, and the AWGN correlation properties are ($\langle \ldots \rangle$ means averaging): $\langle \eta(t,z) \rangle = 0$,

$$\langle \eta(t,z)\bar{\eta}(t',z') \rangle = 2\Gamma\,\delta(t-t')\,\delta(z-z').\tag{49}$$

The AWGN intensity Γ is expressed through the fiber parameters as [7]:

$$2\Gamma = h\,\nu_0\,n_{sp}\,K_T\chi\,,$$

where χ is the fiber loss coefficient, typically typically $\chi \sim 0.2$dB/km, K_T is the temperature-dependant factor (related to the phonon-occupancy factor) that characterizes the Raman pump providing the distributed gain; for the fiber-optic communication systems in normal conditions K_T is close to unity, $K_T = 1.1 \div 1.2$; n_{sp} is the spontaneous emission factor, usually $n_{sp} = 1.3 \div 1.6$; ν_0 is the carrying frequency of the signal, we take it to be $\nu_0 = 193.55$THz. Taking these typical values of parameters, one estimates the order of characteristic noise intensity to be $\Gamma \sim 10^{-21} \div 10^{-20}$. When proceeding to normalized time and distance, Subsection 2.1, the normalized noise intensity D scales as follows: $D = \Gamma\gamma Z_s^2/T_s$.

Now, to study how the noise influences the interrelation of errors associated with the pre-compensated and undistorted signal, we take the example input from Subsection 5.2: 3 slots of 10-mode QPSK-OFDM with the same parameters as were used in Fig. 5, and launch the undistorted and precompensated inputs into noisy channel (48). As there possibly exists a very small probability that for certain critical values of signal amplitude the addition of noise can cause creation of solitonic components in the received signal, one must chose the signal amplitude even weaker than the singularity condition; however, this situation is, generally, highly unlikely as the addition of noise usually arrests the creation of new solitons rather than helps it [44, 45, 48]. However we note that, when performing the Monte-Carlo simulations of signal propagation in noisy model, Eq. (48), and evaluating average errors over several runs (i.e. over several realizations of the AWGN $\eta(z,t)$), each randomly-coded set of OFDM coefficients $c_{\alpha k}$ used in a certain run produces its own particular input profile $q(t)$ and, hence, its own respective output error picture. Because of this the average local absolute error, like the one depicted in Fig. 5, is not informative, as its profile strongly depends on the particular realization of $c_{\alpha k}$ and, thus, disguises the ASE-induced distortions themselves. Therefore we take the *integral*

absolute error for each particular realization of $c_{\alpha k}$ as the measure of signal corruption (here the corruption occurs already due to both noise influence and nonlinearity). For the 3 OFDM slots it means that we take the integral of local absolute error (the error definition is given in Subsection 5.1) over the full signal extent, i.e. from -1.5 to 1.5 in normalized time, evaluating it for precompensated and undistorted inputs separately (see Fig. 5). Next we evaluate the average of this quantity over several runs as a function of i) noise intensity Γ and ii) propagation length L.

The results of our simulations are shown in Fig. 7, where the averaging over 50 realizations was made for each point and we plotted separate graphs for $L = 2000$km, Fig. 7(a), and $L = 4000$km, Fig. 7(b). One can observe that even for the noisy channel the transmission based on the precompensated signal *outperforms* the ordinary transmission (the linear dispersion at the end point was, as before, removed): the average integral absolute error associated with the precompensated inputs (red dots) is lower than that for the non-preprocessed inputs (black squares) for every value of the noise intensity Γ studied. We notice, however, that as far as we operate in the quasilinear regime, the transmission is effectively noise-dominated, so that the nonlinearity induced absolute error, compensated by the preprocessing, is several times lower than the noise-induced error even for the lowest value of noise intensity used, $2\Gamma = 10^{-21}$. In spite of this, the usage of precompensation obviously contributes towards the improvement of the transmission and decrease of distortions in the noisy channel, and our method *is robust against the ASE-induced corruption*.

6.3. General remarks on the NS-based transmission.

In our current study, due to the validity requirements of our spectra equalization method, Section 3, we have addressed the case of quasilinear transmission, where the power of the input is sufficiently low and soliton formation is arrested. However, we want to emphasize that even if the nonlinearity strength and pattern length are such that a simple perturbation-based approach of Section 3 fails, the general idea of the transmission based on NS can still have a significant practical advantage over split-step back-propagation (BP) compensation schemes [16]. Indeed, in any split step back-propagation scheme the number of operations needed for one elementary step scales as $N \log N$ (where N is the resolution in time domain). This, however, is compounded by the need to adjust the coordinate step to compensate for the nonlinear phase shift (this is particularly important for the high pulse power), so that the total number of operation scales as $M \cdot N \cdot \log N$, where $M \gg 1$ is the number of coordinate steps that grows linearly with distance and signal power. In the IST scheme the propagation of the spectral data is the trivial phase rotation so $M = 1$ always, independent of nonlinearity or initial power. As for the direct and inverse NFT, the former requires solving the ZS problem (5) (or a first order Ricatti equation for the scattering coefficient, see e.g. [45]): well-developed methods based on e.g. the piece-wise linear approximation (peeling) of the input $q(t)$ [51] usually take order of N^2 operations. Other methods, based on the reformulation of ZS problem (5) as a matrix eigenvalue problem (see e.g. the part II of [30]), can require a larger number of operations but provide some advantages in the accuracy or more efficiency in the search for complex ZS eigenvalues (solitons). Note that the processing schemes utilizing the NFT have already been proposed [52, 53], although those rather dealt with complex ZS eigenvalues responsible for solitons.

The inverse NFT can be solved using $\sim N^2$ operations, by employing fast Gelfand-Levitan-Marchenko solvers, see e.g. [54] and references therein. So the computational speed-up of the NFT over conventional split step BP is $\sim (M \log N)/N$ operations. To make a real world estimate we have chosen the latest state-of-the-art massively parallel simulations recently reported in [55] with $N = 2^{11}$ and $M = 8000$. Even with the reported impressive speed-up of 30 due to highly efficient parallel algorithm used in the above paper, the potential speed-up of the fully

numerical NFT scheme is still $8000 \times 11/(30 \times 2^{11}) \approx 1.5$, i.e. even in the quasilinear regime and for a relatively small number of z-steps considered in [55], a simple serial numerical NFT-based scheme performs at least as good as a massively parallel direct propagation algorithm. And at higher values of nonlinearity where the required number of coordinate steps, M, is about to grow, the potential effectiveness of the NFT-based modelling schemes is likely to increase. What is most important here is the fact that both algorithms for direct and inverse NFT can be modified to include the appearance of discrete spectra at no extra computational cost. This certainly proves the viability of NFT even beyond the domain of validity of perturbative iteration scheme proposed in Section 3.

Finally we notice that the matrix methods for both the ZS problem [53], and for the GLM equations [54] can be effectively reduced to the Toeplitz matrix inversions. There already exist "superfast" stable algorithms allowing one to perform the Toeplitz matrix inversion by using only $\sim N \log N$ operations [56,57]. Therefore, in view of the arguments given above, we believe that the NFT-based processing and transmission methods can be highly competitive, no less effective than ordinary BP, and even seriously outperform the traditional split-step BP processing.

One of the ideas that allows one to use an encoded continuous NS at larger powers, i.e. when the iterative approach of Section 3 does not rapidly converge failing to produce the correct approximation of NS in a small number of steps, can be the method of *nonlinear inverse syntheses*. The strategy of this method is similar to that widely used in the fiber Bragg gratings design [54]: one starts from the given (encoded) NS profile in the spectral domain (and corresponding reflection coefficient $r(\xi)$, Eq. (7)) and then reconstructs the corresponding profile in time domain by employing the backward NFT, i.e. by solving the corresponding GLM equation. For the focusing NLSE in the absence of discrete ZS spectrum (solitons), the GLM equation (in normalized units) has the form [26–28]:

$$K(t,t') + \bar{F}(t+t') - \int_t^\infty \int_t^\infty K(t,\lambda) F(\lambda+\sigma) \bar{F}(\sigma+t') \, d\sigma \, d\lambda = 0. \qquad (50)$$

Here $F(t)$ designates the backward linear FT of $r(\xi)$ (or of $R(L,\xi)$, if one is interested in the solution at distance L); having solved GLM equation (50) for $K(t,t')$, the sought profile in time domain is eventually recovered as $q(t) = -2K(t,t')|_{t' \to t}$. After the particular form of $q(t)$ corresponding to the encoded NS has been found, one launches this profile into the NLSE. At the receiver we read the output field $q(t,L)$, perform the forward NFT, thus getting the NS $N(\omega;L)$, wind out the accumulated dispersion, and recover the information encoded *without nonlinearity-induced distortions*. The detailed analysis of this approach is beyond the scope of this paper and will be published elsewhere.

7. Conclusion

In this paper, we have examined an application of the inverse scattering transform (nonlinear Fourier transform) to digital signal processing in the coherent communication channel modeled by the integrable NLSE channel. We have demonstrated that the *nonlinear spectrum* (NS) associated with this channel can be used for the improvement of the quality of long-haul information transmission. Without loss of generality, we have illustrated the use of the NS in the case of the OFDM-coded signal. The advantage of using the NS is that the encoded spectral content undergoes just a trivial transformation, similar to the dispersive evolution of spectral component in the linear problem. We would like to stress that the linear spectrum in a nonlinear channel is distorted and its evolution differs drastically from the evolution in a linear dispersive channel. In contrast, the change in the spectral phase of the NS can be easily eliminated at the receiver side, and thus, the informational content can be straightforwardly restored.

To explain the method, we first calculated analytically the NS in the case of a single tone of OFDM and studied the threshold for the nucleation of solitons. We demonstrated that the

threshold in the considered case coincided with that for a pure rectangular pulse of the same energy. For the general situation of several OFDM slots serving as an NLSE input, we showed that NS is qualitatively close to the linear signal spectrum when the energy of the signal is below the soliton-creation threshold: In this situation, the NS can be used for information encoding in the same way as we do with the linear spectrum. The important nontrivial point here is a calculated nonlinear correction to the linear spectrum.

The approach considered in our paper allows one to perform consecutive elimination of the nonlinearity-induced interference effects appearing during the transmission through a nonlinear channel, when the input energy of the single information-carrying pulse is not very high. When the input energy of the pulses block is above the soliton threshold, a more sophisticated modulation can be needed, e.g. separation of small individual information-bearing blocks, such that the shape-sensitive soliton creation threshold is not reached; but the straightest way in this case is to employ the inverse syntheses method briefly described at the end of Subsection 6.3.

Using the expansion of the NS, we propose the *nonlinear pre-distortion technique*, which allows one to *equalize* the NS with the linear spectrum of the undistorted input signal. Then, the informational content encoded on the NS can be recovered at the receiver with standard linear methods after the linear accumulated dispersion has been compensated. We found that our technique worked well even for a relatively long OFDM sequence, provided that the input pulse does not nucleate a soliton. We have also demonstrated that our approach is general and works well also for the Gaussian-based WDM input, where the NS expansion cannot be computed analytically. Further, we analyzed the robustness of our approach against the noise associated with amplifier spontaneous emission and revealed that even though the quasilinear regime is noise-dominated, the average error associated with the pre-compensated inputs is always lower than that for non-processed transmission. We hope that our work represents an important first step in the development of efficient digital signal techniques based on the inverse scattering transform capable of eliminating nonlinear distortion of the optical signal in the NLSE channel via pre- or post-processing using the integrability of the NLSE (2). The forward NFT itself consists in the solution of just the linear system – the ZS spectral problem (5). We note that the squares of ZS eigenfunctions (Jost solutions) constitute an orthogonal basis (5), and this paves the way for various perturbative approaches for the consideration of noise influence and other nearly-integrable (weakly perturbed NLSE) cases. We anticipate that with the further development of practical implementation of the proposed approaches, certain nonlinear fiber communication channels can be effectively linearized. The numerical complexity of the transmission based on NS and, generally, of the NFT-based methods, can be of the same order of even lower than that for traditional slit-step back propagation.

Acknowledgments